

Duke University  
Department of Mathematics

Senior Honors Thesis  
Spring 2008

Existence and Stability of Patterns Arising from Square  
Wave Forcing of the Damped Mathieu Equation

Michael Edward Bauer  
Advisor: Dr. Anne Catllá  
Submitted: April 23, 2008

This work was supported by an NSF VIGRE grant (NSF-DMS-9983320) and a  
PRUV Fellowship from the Duke University Department of Mathematics.

## Abstract

In this work the nature and stability of patterns arising from parametric square-wave forcing of an inviscid fluid layer of infinite depth are investigated. Specifically the case of vertically shaken fluids is considered. Beginning with the non-linear PDE's of the Zhang-Viñals Model of a fluid surface under small perturbations, it is shown how a linear, second order ODE damped Mathieu equation arises from a linear stability analysis. This analysis is performed for several different square wave forcing functions. It is shown both analytically and in the neutral stability curves that square wave forcing can be reduced to delta function forcing in the appropriate limit. In addition to this, the effects of larger forcing times on the neutral stability curves are examined. The effect of fluid parameters on the neutral stability curves is also explored. Lastly, a numerical solver is developed to observe the different patterns that are generated by several configurations of square wave forcing.

# Contents

<b>1</b>	<b>Introduction</b>	<b>4</b>
<b>2</b>	<b>Determining the Stability of Faraday Waves</b>	<b>5</b>
2.1	Derivation of the Mathieu Equation from the Zhang-Viñals Model via Linearization . . . . .	5
2.2	Floquet Multipliers and Solution Stability . . . . .	6
<b>3</b>	<b>Square Wave Forcing of the Mathieu Equation</b>	<b>7</b>
3.1	Calculation . . . . .	7
3.2	Approximating Delta Function Forcing . . . . .	9
3.3	Examining Instabilities with Larger $r$ . . . . .	12
<b>4</b>	<b>Alternating Square Wave Forcing</b>	<b>12</b>
4.1	Calculation . . . . .	12
4.2	Approximating Alternating Delta Function Forcing . . . . .	15
4.3	Instabilities with Larger $r$ Values . . . . .	16
<b>5</b>	<b>Inverted Square Wave Forcing</b>	<b>18</b>
<b>6</b>	<b>Impact of Fluid Parameters on Neutral Stability Curves</b>	<b>20</b>
6.1	Impact of $G_0$ and $\Gamma_0$ . . . . .	23
6.2	Impact of $\gamma$ . . . . .	26
<b>7</b>	<b>Visualizing Pattern Formation</b>	<b>26</b>
7.1	Numerical Methods . . . . .	28
7.2	Patterns Arising from Square Wave Forcing . . . . .	30
7.3	Patterns Arising from Alternating Square Wave Forcing . . . . .	31
7.4	Understanding Pattern Formation Under Square Wave Forcing . . . . .	32
<b>8</b>	<b>Future Work</b>	<b>33</b>
<b>9</b>	<b>Conclusions</b>	<b>34</b>

# 1 Introduction

Recently the idea of trying to understand pattern formation has been appearing in many fields: in computer science machine learning looks to develop means of having computers recognize patterns, in neuroscience researchers are looking to understand how people recognize patterns, and in biology scientists are studying how patterns form in different natural systems. Indeed it is interesting to see the many broad applications that can be classified as understanding pattern formation. However, despite our ability to describe and classify patterns, very little is known about the underlying causes of patterns. In this work we hope to contribute an understanding of the fundamental nature of patterns resulting from systems undergoing parametric forcing.

Parametrically forced fluids were first studied by Faraday in [1] and have consequently been referred to as Faraday systems ever since. In Faraday systems the forcing of the system is not independent of the current state of the system. Instead the system is said to undergo parametric forcing where the forcing function is coupled to the current state of the system in some way. Interestingly different experiments have shown that there exists a rich variety of patterns that can be generated using different forcing functions and media. In this work we investigate the stability and types of patterns that form as a result of parametrically exciting the surface of a fluid. In these experiments the system consists of a fluid that is vertically shaken, potentially generating patterns on the surface. Note that in this case the forcing function is used to define the acceleration of the system and not its position.

One of the most interesting properties of Faraday waves (patterns forming in Faraday systems) is that they often exhibit a frequency that is half of the frequency of the forcing function. This type of response is referred to as a subharmonic response as it represents a resonance that is at a frequency below the forcing frequency. This result was first explained by Benjamin and Ursell who demonstrated that an ideal fluid undergoing parametric forcing could be described by a Mathieu equation [13]. While this provided some insight into the causes of subharmonic forcing, there was no model for describing the patterns that could form on the surface of a fluid until Zhang and Viñals proposed their quasi-potential model [2]. This model describes the behavior of a weakly viscous fluid layer without having to model the entire bulk fluid using the Navier-Stokes equations. The Zhang-Viñal's model captures the behavior of the fluid surface by describing both its amplitude (usually denoted by  $h$ ) and a surface velocity potential (usually denoted by  $\Phi$ ) that describes how  $h$  will be updated. In this work we employ the Zhang-Viñal's model both to begin our analysis and in our fluid simulation experiment.

Traditionally most experiments that looked at the patterns generated by parametric forcing utilized some sinusoidal or multi-frequency forcing. Two-frequency forcing has experimentally generated many patterns including superlattice pat-

ters [8], quasi-patterns [10], triangular patterns [11], and local structures [12]. Similarly, Topaz, Porter, and Silber investigated the theoretical causes of different patterns arising from multi-frequency forcing [9]. It has only been recently that non-smooth forcing functions have begun to be explored. Bechhoefer and Johnson first explored the patterns generated by a sequence of periodic delta functions [4]. Catllá, Porter, Silber then extended the work of Bechhoefer and Johnson by examining the weakly non-linear effects that can occur under impulse forcing functions [6]. In this particular work we begin to examine a new class of non-smooth forcing functions: square waves.

Beginning with the derivation of the damped Mathieu equation from the Zhang-Viñals model, we show how to solve for the neutral stability curves of different square wave forcing functions. We also demonstrate that our result reduces to the case of delta function forcing in the limit as the time spent forcing is taken to zero. This shows that square wave forcing is a more general form of delta function forcing. We then examine the impact of different fluid and forcing parameters on the neutral stability curves. Lastly, we develop a numerical solver for the partial differential equations of the Zhang-Viñals model in order to observe the various patterns that form as a result of square wave forcing.

## 2 Determining the Stability of Faraday Waves

### 2.1 Derivation of the Mathieu Equation from the Zhang-Viñals Model via Linearization

The Zhang-Viñals model of the Faraday problem may be derived directly from the Navier-Stokes equations. By assuming fluid flow in the bulk is potential, Zhang and Viñals were able to show in [2] that surface height  $h(\mathbf{x}, t)$  and surface velocity potential  $\Phi(\mathbf{x}, t)$  were solutions to the boundary conditions given by

$$(\partial_t - \gamma \nabla^2)h - \hat{D}\Phi = N_1(h, \Phi), \quad (1a)$$

$$(\partial_t - \gamma \nabla^2)\Phi - [\Gamma_0 \nabla^2 - G_0 + G(t)]h = N_2(h, \Phi), \quad (1b)$$

where the nonlinear terms in (1) are defined as

$$\begin{aligned} N_1(h, \Phi) = & -\nabla \cdot (h \nabla \Phi) + \frac{1}{2} \nabla^2 (h^2 \hat{D}\Phi) \\ & - \hat{D}(h \hat{D}\Phi) + \hat{D} \left[ h \hat{D}(h \hat{D}\Phi) + \frac{1}{2} h^2 \nabla^2 \Phi \right], \end{aligned} \quad (2a)$$

$$\begin{aligned} N_2(h, \Phi) = & \frac{1}{2} (\hat{D}\Phi)^2 - \frac{1}{2} (\nabla \Phi)^2 \\ & - \frac{1}{2} \Gamma_0 \nabla \cdot [(\nabla h)(\nabla h)^2] - (\hat{D}\Phi) \left[ h \nabla^2 \Phi + \hat{D}(h \hat{D}\Phi) \right]. \end{aligned} \quad (2b)$$

In the above equations the operator  $\hat{D}$  performs the operation of multiplying each Fourier component by its wave number, e.g.  $\hat{D}e^{i\mathbf{k}\cdot\mathbf{x}} = |\mathbf{k}|e^{i\mathbf{k}\cdot\mathbf{x}}$ , and the dimensionless parameters are

$$\gamma \equiv \frac{2\nu k_0^2}{\omega}, \quad \Gamma_0 \equiv \frac{\Gamma k_0^3}{\rho\omega^2}, \quad G_0 \equiv \frac{gk_0}{\omega^2}, \quad (3)$$

where  $g$  is the acceleration due to gravity,  $\omega$  is the forcing frequency,  $\nu$  is the kinematic viscosity,  $\rho$  is the density, and  $\Gamma$  is the surface tension. Since we have assumed an inviscid fluid, the parameter  $k_0$  must satisfy the dispersion relation

$$gk_0 + \frac{\Gamma k_0^3}{\rho} = \left(\frac{\omega}{2}\right)^2. \quad (4)$$

By dividing this equation by  $\omega^2$  we arrive at the relation  $G_0 + \Gamma_0 = \frac{1}{4}$ .

The next step in the analysis is to demonstrate that the linearization of the Zhang-Viñals equations reduces to the damped Mathieu equation. We begin by linearizing the Zhang-Viñals equations by setting all the non-linear terms in (2) to zero. This leaves us with a system of coupled partial differential equations. We assume that this system has solutions of the form  $h(\mathbf{x}, t) = p_k(t)e^{i\mathbf{x}\cdot\mathbf{k}} + \text{c.c.}$  and  $\Phi(\mathbf{x}, t) = q_k(t)e^{i\mathbf{x}\cdot\mathbf{k}} + \text{c.c.}$  where c.c. denotes the complex conjugate of the preceding term. Substituting these forms into (1) we see that the eigenfunctions  $p_k(t)$  must satisfy the damped Mathieu equation

$$\ddot{p}_k + 2\gamma k^2 \dot{p}_k + [\gamma^2 k^4 + \Gamma_0 k^3 + (G_0 - G(t))k]p_k = 0 \quad (5)$$

where  $k = |\mathbf{k}|$ . Contrary to direct forcing of a system where the forcing function is a non-homogeneous component of the equation, e.g.  $\ddot{x} + \gamma\dot{x} + \omega^2 x = G(t)$ , the damped Mathieu equation represents parametric forcing. With parametric forcing, both the current state of the system as well as the forcing function determine the response of the system. It is this property that leads to both stable and unstable solutions to the Mathieu equation.

For our study we have chosen to examine the effects of square wave forcing on the Mathieu equation. By modulating different parameters of the square wave we will be able to determine the neutral stability curves where the solutions of the Mathieu equation transition from being stable to unstable.

## 2.2 Floquet Multipliers and Solution Stability

In order to determine the stability of solutions to the Mathieu equation we will utilize Floquet theory [3]. Floquet theory deals primarily with determining the periodicity of the solution given that the fundamental matrix for a system is periodic.

**Floquet's theorem.** *Given a system  $\dot{\mathbf{x}} = \alpha\mathbf{P}(t)\mathbf{x}$  where  $\mathbf{P}$  is an  $n \times n$  matrix with minimal period  $T$  and  $\alpha$  is a constant, then the system has at least one*

non-trivial solution  $\mathbf{x} = \boldsymbol{\chi}(t)$  such that

$$\boldsymbol{\chi}(t + T) = \mu \boldsymbol{\chi}(t) \quad (6)$$

where  $\mu$  is constant.

For a full proof of this theorem see [3]. The constant  $\mu$  described in Floquet's theorem is called a Floquet multiplier. We are particularly interested in the nature of these Floquet multipliers as certain values will assure that the solution of the system is periodic.

We now assert without proof that the solutions of the system are periodic whenever the Floquet multipliers satisfy the following condition

$$\mu = 1^{\frac{1}{m}} \quad (7)$$

where  $m$  is a positive integer. For a complete derivation of this statement see [3]. It has been shown [14] that the transition from the flat fluid state to Faraday waves occurs only for real valued Floquet multipliers,  $\mu \pm 1$ . These are the exact conditions that [4] utilize for determining the stability of solutions to the Mathieu equation. Armed with these tools we can now attack the problem of determining the stability of solutions to the damped Mathieu equation for square wave forcing.

### 3 Square Wave Forcing of the Mathieu Equation

#### 3.1 Calculation

Our general forcing function, traditionally referred to as a square wave, is best described as a sum of Heaviside equations (denoted by  $h(t)$ ) represented as

$$G(t) = \epsilon \sum_n h(t - n\Delta t - \Delta t_1) - h(t - n\Delta t - (\Delta t_1 + \Delta t_2)). \quad (8)$$

Here  $\Delta t$  is the period of the square wave,  $\Delta t_1$  is the amount of time during a period that  $G(t)$  is zero, and  $\Delta t_2 = \Delta t - \Delta t_1$ . Figure 1 gives an example a square wave with the different time periods labeled.

We begin by following the method used by [4] to analyze the effect of periodic delta-function forcing. It is important to notice that unlike [4] the square wave forces us to consider two different cases: an instantaneous change in acceleration or "jerk" from zero to  $\epsilon$  and a jerk from  $\epsilon$  back to zero. In between jerks we can assume a solution of the form

$$x_n(t) = A_n e^{\psi(t-t_n)} + \text{c.c.} \quad (9)$$

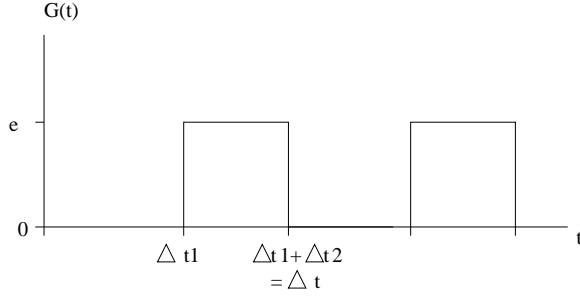


Figure 1: An example of square wave forcing including the definitions for  $\Delta t_1$ ,  $\Delta t_2$ , and  $\Delta t$ .

where c.c. stands for the complex conjugate,  $t_n = n\Delta t$  denotes the time at the beginning of the  $n^{\text{th}}$  period, and  $\psi(t)$  takes the forms of

$$\psi_0(t) = -\gamma k^2 \pm i\Omega(k) \quad (10a)$$

$$\psi_\epsilon(t) = -\gamma k^2 \pm \sqrt{\Omega^2(k) - k\epsilon} \quad (10b)$$

corresponding to when  $G(t)$  is equal to zero and when  $G(t)$  is equal to  $\epsilon$  respectively and  $\Omega^2(k)$  is the dispersion relation

$$\Omega^2(k) = \Gamma_0 k^3 + G_0 k. \quad (11)$$

We know from [5] that the solution at the jerks must satisfy the following conditions

$$x_{n+\frac{1}{2}}(t_{n+\frac{1}{2}}) = x_n(t_{n+\frac{1}{2}}) \quad (12a)$$

$$\dot{x}_{n+\frac{1}{2}}(t_{n+\frac{1}{2}}) = \dot{x}_n(t_{n+\frac{1}{2}}) \quad (12b)$$

where  $t_{n+\frac{1}{2}} = (n + \frac{1}{2})\Delta t$  denotes the time halfway through the  $n^{\text{th}}$  period. By applying these conditions at the two jerks contained in a period we obtain the following maps from  $A_{k,n}$  to  $A_{k,n+1}$

$$\begin{pmatrix} A_{k,n+\frac{1}{2}}^r \\ A_{k,n+\frac{1}{2}}^i \end{pmatrix} = e^{-\gamma k^2 \Delta t_1} \begin{pmatrix} C_1 & -S_1 \\ \alpha S_1 & \alpha C_1 \end{pmatrix} \begin{pmatrix} A_{k,n}^r \\ A_{k,n}^i \end{pmatrix} = e^{-\gamma k^2 \Delta t_1} M_{1,k} \begin{pmatrix} A_{k,n}^r \\ A_{k,n}^i \end{pmatrix} \quad (13a)$$

$$\begin{pmatrix} A_{k,n+1}^r \\ A_{k,n+1}^i \end{pmatrix} = e^{-\gamma k^2 \Delta t_2} \begin{pmatrix} C_2 & -S_2 \\ \alpha^{-1} S_2 & \alpha^{-1} C_2 \end{pmatrix} \begin{pmatrix} A_{k,n+\frac{1}{2}}^r \\ A_{k,n+\frac{1}{2}}^i \end{pmatrix} = e^{-\gamma k^2 \Delta t_2} M_{2,k} \begin{pmatrix} A_{k,n+\frac{1}{2}}^r \\ A_{k,n+\frac{1}{2}}^i \end{pmatrix} \quad (13b)$$

corresponding to when  $G(t)$  transitions from zero to  $\epsilon$  ( $M_{1,k}$ ) and when  $G(t)$  transitions from  $\epsilon$  to zero ( $M_{2,k}$ ) respectively. In the above equations  $A_{k,n}^r$  ( $A_{k,n}^i$ ) is the real (imaginary) part of  $A_{k,n}$  and  $C_1 \equiv \cos(\Omega(k)\Delta t_1)$ ,  $S_1 \equiv \sin(\Omega(k)\Delta t_1)$ ,  $C_2 \equiv \cos(\sqrt{\Omega^2(k) - k\epsilon}\Delta t_2)$ ,  $S_2 \equiv \sin(\sqrt{\Omega^2(k) - k\epsilon}\Delta t_2)$ ,  $\alpha \equiv \frac{\Omega(k)}{\sqrt{\Omega^2(k) - k\epsilon}}$ .

By combining these two maps we then create a map ( $M_k = M_{2,k}M_{1,k}$ ) across one period of the square wave

$$\begin{pmatrix} A_{k,n+1}^r \\ A_{k,n+1}^i \end{pmatrix} = e^{-\gamma k^2 \Delta t} M_{2,k} M_{1,k} \begin{pmatrix} A_{k,n}^r \\ A_{k,n}^i \end{pmatrix}. \quad (14)$$

The eigenvalues of  $M_k$  are the Floquet multipliers of the system and will be used to determine the stability of the system. Since we know that  $(\det M_k) = (\det M_{2,k})(\det M_{1,k}) = \alpha^{-1}\alpha = 1$  we can define the Floquet multipliers

$$\lambda_{\pm} = \frac{1}{2} \text{Tr}(M_k) \pm \sqrt{\left[ \frac{1}{2} \text{Tr}(M_k) \right]^2 - 1}. \quad (15)$$

Whenever both of the Floquet multipliers are real and the magnitude of the largest is greater than  $e^{-\gamma k^2 \Delta t}$  then the system is unstable. This results in a threshold condition of

$$\frac{1}{2} \text{Tr}(M_k) = \pm \cosh(\gamma k^2 \Delta t). \quad (16)$$

In the above condition the “+” corresponds to a harmonic instability while the “-” represents a subharmonic instability in  $\epsilon(k)$ . From this condition we can derive an implicit equation  $f(\Delta t, k, \epsilon) = \pm \cosh(\gamma k^2 \Delta t) - \frac{1}{2} \text{Tr}(M_k) = 0$  which cannot be solved explicitly for  $\epsilon(k)$ , but can be solved numerically. The curves created by numerically solving the equation are referred to as the neutral stability curves. The neutral stability curves lie on the boundary between stable and unstable regions and form a sequence of tongues as can be seen in Figure 2. The regions inside of the tongues are considered to be places where stable patterns are capable of forming while the regions outside of the tongues do not contain enough energy to support stable pattern formation. Outside of the tongues only the trivial (flat) solution is stable. The nature of the neutral stability curves provides us with fundamental information concerning the conditions necessary for stable patterns to form and will be central to our study.

### 3.2 Approximating Delta Function Forcing

The next step in our analysis is to demonstrate that by changing the relative magnitudes of  $\Delta t_1$  and  $\Delta t_2$  we can approximate the results obtained in [4] for delta function forcing. We define

$$r = \frac{\Delta t_2}{\Delta t} \quad (17)$$

to be the ratio of the period that the square wave remains at  $\epsilon$ . By gradually decreasing the value of  $r$  until  $r \rightarrow 0$  we can achieve a square wave approximation to delta function forcing.

We can show analytically that under the limit  $\Delta t_1 \rightarrow \Delta t$  and  $\Delta t_2 \rightarrow 0$ , our result is equivalent to the one obtained in [4] for delta function forcing. Since  $\Delta t_2$  is being taken as the limit goes to zero, we can apply a first order Taylor series expansion for the corresponding sine and cosine, thereby leaving us with the following threshold condition.

$$\pm \cosh(\gamma k^2 \Delta t) = \cos(\Omega(k) \Delta t) - \frac{1}{2} \sin(\Omega(k) \Delta t) \sqrt{\Omega^2(k) + k \epsilon \Delta t_2} (\alpha + \alpha^{-1}) \quad (18)$$

After some algebraic manipulation we arrive at

$$\Omega(k) \Delta t_2 + \frac{k \epsilon \Delta t_2}{2 \Omega(k)} = \frac{\cos(\Omega(k) \Delta t) \pm \cosh(\gamma k^2 \Delta t)}{\sin(\Omega(k) \Delta t)} \quad (19)$$

Here we notice that the term  $\epsilon \Delta t_2 \equiv \hat{\epsilon}$  which corresponds to the magnitude of the delta function in [4]. After making this substitution we then take the limit as  $\Delta t_2 \rightarrow 0$  and arrive at the same expression as [4] for the neutral stability curves of delta function forcing.

$$\hat{\epsilon}_c(\Delta t) = \frac{2 \Omega(k)}{k} \left( \frac{\cos(\Omega(k) \Delta t) \pm \cosh(\gamma k^2 \Delta t)}{\sin(\Omega(k) \Delta t)} \right) \quad (20)$$

By plotting the neutral stability curves for different values of  $r$ , as can be seen in Figure 2, we notice that curves become increasingly asymmetric as  $r \rightarrow 0$ . The curves whose minima form at odd values of  $k$  are subharmonic tongues while those on even values are harmonic tongues. Recall that subharmonic tongues refer to locations where patterns would form with frequencies that are odd multiples of half of the forcing frequency and that the harmonic tongues correspond to even multiples of half of the forcing frequency. It should be noted here that we have plotted the neutral stability curves as a function of  $k$  and not  $\Delta t$  as done in [4]. In this paper we have non-dimensionalized around  $\Delta t$  so that the forcing function will always have a dimensionless period of  $2\pi$ . However, plotting versus  $k$  and versus  $\Delta t$  are equivalent as shown by the following equation involving the dispersion relation.

$$\Delta t = \frac{2\pi}{\Omega(k)} \quad (21)$$

When comparing the results above to the results obtained in [4] it is important to recognize that the amplitude of the delta function,  $\hat{\epsilon}$ , is defined by our convention to be

$$\hat{\epsilon} \equiv \epsilon \Delta t_2 = \epsilon r \Delta t. \quad (22)$$

This difference is important when comparing the amplitudes of the minimum for each tongue. [4] indicates the values of  $\epsilon$  to be much smaller than demonstrated by our graphs. However, if each minimum is multiplied by  $r \Delta t$  then the results provide a more accurate approximation of the results obtained in [4].

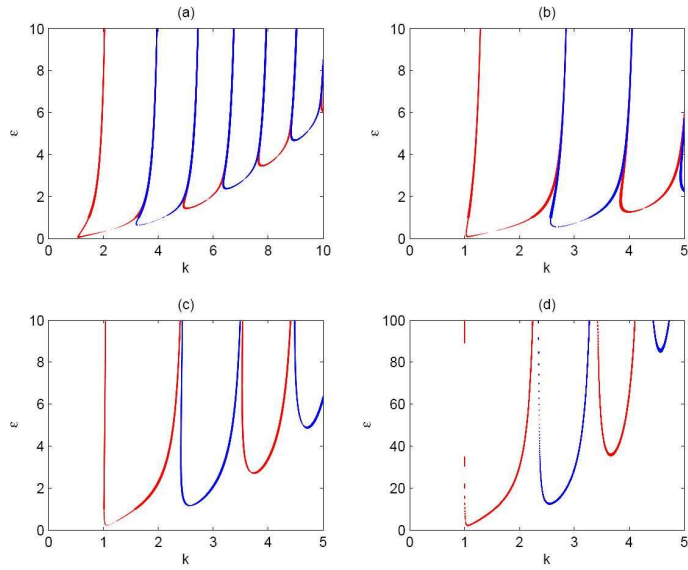


Figure 2: Neutral stability curves for square wave forcing designed to approximate delta function forcing. Red corresponds to subharmonic tongues and blue corresponds to harmonic tongues. The ratio of the square waves  $r$  as defined in (17) is (a)  $r = 0.5$ , (b)  $r = 0.25$ , and (c)  $r = 0.1$ . Example (d) is identical to example (c) except the values of  $\epsilon$  have been scaled to the values of  $\hat{\epsilon}$  as defined in (22). The dimensionless parameters used in these examples are  $\gamma = 0.02$  and  $\Gamma_0 = 0.040$  (corresponding to fluid parameters  $\nu=0.02$  cm<sup>2</sup>/s,  $\Gamma=1.87$  dyn/cm,  $\rho=1$  g/cm<sup>3</sup>, and  $\omega/2\pi=34$  Hz). The fluid parameters used in this system are maintained throughout all of the following examples.

Another important consideration to take into account when comparing the above results to [4] is the physical significance of the sign of  $G(t)$  as defined in the Mathieu equation. In our definition positive forcing corresponds to moving opposite the force of gravity. In [4] positive forcing is defined to be in the same direction as gravity since the sign preceding the  $g(t)x$  terms is positive instead of negative.

$$\ddot{x} + 2\gamma\dot{x} + \omega_0^2[1 + g(t)]x = 0 \quad (23)$$

This accounts for the reflection of each tongue about its asymptote in comparison to [4].

### 3.3 Examining Instabilities with Larger $r$

In the previous section we showed that for small values of  $r$  the square wave becomes a very good approximation of delta function forcing. In this section we examine what happens to the neutral stability curves as  $r \rightarrow 1$ .

Notice that in the case that the values of  $r$  increase the system will spend a larger portion of time accelerating opposite of gravity while at the same time spending less time maintaining a constant velocity. This implies that energy is being added to the system at a much higher rate than the approximate delta function forcing examined earlier.

From the plots shown in Figure 3 we can see that as the value of  $r$  is increased the tongues begin to widen, but still maintain the minimum at around the same value of  $k$  as they did in the approximate delta function forcing analysis. In order to accomplish this, the tongues end up “curling” underneath each other. In addition to this, the minimum of the tongues increases with larger  $r$  value in a non-linear manner. In Figure 3(d) this is clearly visible as the minimum of the second subharmonic tongue is not even visible even at values of  $\epsilon$  around 40. This result is an interesting one as it shows that as we increase the amount of time the system spends accelerating, we increase the width of the instabilities, pushing up the minima of higher order tongues, thereby indicating that lower and lower values of  $\epsilon$  are required to make the system unstable.

## 4 Alternating Square Wave Forcing

### 4.1 Calculation

We now modify our square wave forcing function so that it contains both positive and negative components in alternating series. This function can be expressed as

$$G(t) = \epsilon \sum_n h(t - n\Delta t - \Delta t_1) + h(t - n\Delta t - (\Delta t_1 + \Delta t_2 + \Delta t_3 + \Delta t_4)) - h(t - n\Delta t - (\Delta t_1 + \Delta t_2)) - h(t - n\Delta t - (\Delta t_1 + \Delta t_2 + \Delta t_3)) \quad (24)$$

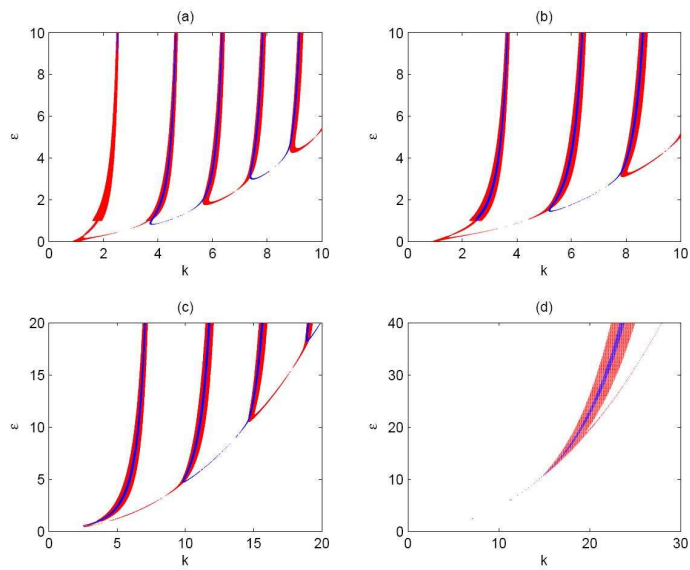


Figure 3: Examples of square wave forcing for larger values of  $r$ . The values for the corresponding plots are as follows: (a)  $r = 0.6$ , (b)  $r = 0.75$ , (c)  $r = 0.9$ , (d)  $r = 0.99$ . Notice how as the value of  $r$  increases the width of the tongues continues to increase. The minima of the tongues also continue to grow as  $r$  is increased. Please note that the appearance of some tongues fading out or appearing artificially wide is only an artifact of our numerical plotter and does not reflect their existence or actual size.

In the above equation  $\Delta t$  is still the period of the square wave.  $\Delta t_2$  represents the time during one period that  $G(t)$  is equal to  $\epsilon$  and  $\Delta t_4$  represents the time during one period that  $G(t)$  is equal to  $-\epsilon$ .  $\Delta t_1$  and  $\Delta t_3$  represent the time spent at zero between the time spent at  $\epsilon$  and  $-\epsilon$ .

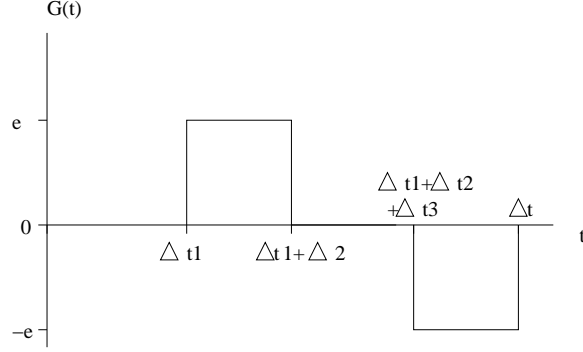


Figure 4: An example of alternating square wave forcing demonstrating the definitions of  $\Delta t_1$ ,  $\Delta t_2$ ,  $\Delta t_3$ ,  $\Delta t_4$ , and  $\Delta t$ .

Using the same method employed earlier we begin by noticing that we must take into account four different conditions: a jerk from zero to  $\epsilon$ , a jerk from  $\epsilon$  to zero, a jerk from zero to  $-\epsilon$ , and a jerk from  $-\epsilon$  to zero. We again assume the solution stated in (9) in between jerks, however in addition to (10),  $\psi(t)$  will also take the form

$$\psi_{-\epsilon}(t) = -\gamma k^2 \pm \sqrt{\Omega^2(k) + k\epsilon} \quad (25)$$

when  $G(t)$  is equal to  $-\epsilon$ . Here  $\Omega^2(k)$  is the same as defined in (11). The conditions that must be satisfied at each jerk remain the same, however we will redefine them here for notational clarity.

$$x_{n+\frac{1}{4}}(t_{n+\frac{1}{4}}) = x_n(t_{n+\frac{1}{4}}) \quad (26a)$$

$$\dot{x}_{n+\frac{1}{4}}(t_{n+\frac{1}{4}}) = \dot{x}_n(t_{n+\frac{1}{4}}) \quad (26b)$$

By applying these conditions at each of the four points of discontinuity we derive the following four maps from  $A_{k,n}$  to  $A_{k,n+1}$

$$\begin{pmatrix} A_{k,n+\frac{1}{4}}^r \\ A_{k,n+\frac{1}{4}}^i \end{pmatrix} = e^{-\gamma k^2 \Delta t_1} \begin{pmatrix} C_1 & -S_1 \\ \alpha S_1 & \alpha C_1 \end{pmatrix} \begin{pmatrix} A_{k,n}^r \\ A_{k,n}^i \end{pmatrix} \quad (27a)$$

$$\begin{pmatrix} A_{k,n+\frac{1}{2}}^r \\ A_{k,n+\frac{1}{2}}^i \end{pmatrix} = e^{-\gamma k^2 \Delta t_2} \begin{pmatrix} C_2 & -S_2 \\ \alpha^{-1} S_2 & \alpha^{-1} C_2 \end{pmatrix} \begin{pmatrix} A_{k,n+\frac{1}{4}}^r \\ A_{k,n+\frac{1}{4}}^i \end{pmatrix} \quad (27b)$$

$$\begin{pmatrix} A_{k,n+\frac{3}{4}}^r \\ A_{k,n+\frac{3}{4}}^i \end{pmatrix} = e^{-\gamma k^2 \Delta t_3} \begin{pmatrix} C_3 & -S_3 \\ \hat{\alpha} S_3 & \hat{\alpha} C_3 \end{pmatrix} \begin{pmatrix} A_{k,n+\frac{1}{2}}^r \\ A_{k,n+\frac{1}{2}}^i \end{pmatrix} \quad (27c)$$

$$\begin{pmatrix} A_{k,n+1}^r \\ A_{k,n+1}^i \end{pmatrix} = e^{-\gamma k^2 \Delta t_4} \begin{pmatrix} C_4 & -S_4 \\ \hat{\alpha}^{-1} S_4 & \hat{\alpha}^{-1} C_4 \end{pmatrix} \begin{pmatrix} A_{k,n+\frac{3}{4}}^r \\ A_{k,n+\frac{3}{4}}^i \end{pmatrix} \quad (27d)$$

corresponding to to when  $G(t)$  transitions from  $0 \rightarrow \epsilon$  ( $M_{1,k}$ ),  $\epsilon \rightarrow 0$  ( $M_{2,k}$ ),  $0 \rightarrow -\epsilon$  ( $M_{3,k}$ ), and  $-\epsilon \rightarrow 0$  ( $M_{4,k}$ ) respectively. In the above equations  $C_1, C_2, S_1, S_2$ , and  $\alpha$  all have the same definitions as before and  $C_3 \equiv \cos(\Omega(k)\Delta t_3)$ ,  $S_3 \equiv \sin(\Omega(k)\Delta t_3)$ ,  $C_4 \equiv \cos(\sqrt{\Omega^2(k) + k\epsilon}\Delta t_4)$ ,  $S_4 \equiv \sin(\sqrt{\Omega^2(k) + k\epsilon}\Delta t_4)$ , and  $\hat{\alpha} = \frac{\Omega(k)}{\sqrt{\Omega^2(k) + k\epsilon}}$ .

Combining the above maps then allows us to create a map ( $M_k = M_{4,k}M_{3,k}M_{2,k}M_{1,k}$ ) over a whole period of square wave

$$\begin{pmatrix} A_{k,n+1}^r \\ A_{k,n+1}^i \end{pmatrix} = e^{-\gamma k^2 \Delta t} M_{4,k} M_{3,k} M_{2,k} M_{1,k} \begin{pmatrix} A_{k,n}^r \\ A_{k,n}^i \end{pmatrix} \quad (28)$$

The eigenvalues of  $M_k$  again are the Floquet multipliers of the system and since  $(\det M_k) = (\det M_{k,4})(\det M_{k,3})(\det M_{k,2})(\det M_{k,1}) = (\hat{\alpha}^{-1})(\hat{\alpha})(\alpha^{-1})(\alpha) = 1$  the Floquet multipliers still have the same form as (15). The same threshold condition as (16) still applies and allows us to again form the implicit equation  $f(\Delta t, k, \epsilon) = \pm \cosh(\gamma k^2 \Delta t) - \frac{1}{2} \text{Tr}(M_k) = 0$ . Solving this equation numerically will allow us to determine the neutral stability curves of the system.

## 4.2 Approximating Alternating Delta Function Forcing

Our next step in the analysis is to show that by modulating the values of  $\Delta t_2$  and  $\Delta t_4$  we can approximate the results obtained in [4] and [6] for alternating delta function forcing. We define

$$r_1 \equiv \frac{\Delta t_2}{\Delta t}, \quad r_2 \equiv \frac{\Delta t_4}{\Delta t} \quad (29)$$

to be the ratio of time per period that  $G(t)$  spends at  $\epsilon$  and  $-\epsilon$  respectively. By taking the limit as  $\Delta t_2, \Delta t_4 \rightarrow 0$  we will be able to obtain an approximation to alternating delta function forcing.

For the purposes of this calculation we will assume that  $\Delta t_1 = \Delta t_3$  (for a more rigorous treatment of what happens when  $\Delta t_1 \neq \Delta t_3$  see [6]). We can verify analytically that under the limit  $\Delta t_2, \Delta t_4 \rightarrow 0$  and  $\Delta t_1, \Delta t_3 \rightarrow \frac{\Delta t}{2}$  alternating square wave forcing becomes alternating delta function forcing. We begin with the same threshold condition described in (16). Since  $M_k$  is the product of four matrices, the algebraic component of this problem becomes extensive. By utilizing the substitutions defined earlier and the fact that  $C_1 \equiv C_3$  and  $S_1 \equiv S_3$

we have

$$\begin{aligned} \pm \cosh(\gamma k^2 \Delta t) &= 2C_1^2 C_2 C_4 - 2\alpha C_1 S_1 S_2 C_4 - 2\hat{\alpha}_2 C_1 S_1 C_2 S_4 + \\ &\quad \left( \alpha \hat{\alpha} + \frac{1}{\alpha \hat{\alpha}} \right) S_1^2 S_2 S_4 + \left( \frac{\alpha}{\hat{\alpha}} + \frac{\hat{\alpha}}{\alpha} \right) C_1^2 S_2 S_4 + \\ &\quad - 2S_1^2 C_2 C_4 - \frac{2}{\alpha} C_1 S_1 S_2 C_4 - 2\frac{2}{\hat{\alpha}} C_1 S_1 C_2 S_4. \end{aligned} \quad (30)$$

Since  $\Delta t_2, \Delta t_4 \rightarrow 0$  we can substitute a first order Taylor series expansion for  $C_2, S_2, C_4,$  and  $S_4$ . By making this substitution, taking the limit for all terms not containing  $\epsilon$ , and simplifying terms, we arrive at the much simpler expression

$$\frac{1}{2} \left( \frac{2\Omega^4(k) - k^2 \epsilon^2}{\Omega^2(k)} \right) S_1^2 \Delta t_2 \Delta t_4 = \pm \cosh(\gamma k^2 \Delta t) - C_1^2 + S_1^2. \quad (31)$$

We then recognize that  $\epsilon \Delta t_2 \equiv -\epsilon \Delta t_4 \equiv \hat{\epsilon}$ . After making this substitution and taking the limit as  $\Delta t_2, \Delta t_4 \rightarrow 0$  we have the following expression

$$\frac{1}{2} \frac{k^2 \hat{\epsilon}^2}{\Omega^2(k)} S_1^2 = \pm \cosh(\gamma k^2 \Delta t) - C_1^2 + S_1^2. \quad (32)$$

After some algebraic manipulation we arrive at the following expression which is identical to the expression obtained in both [4] and [6] for alternating delta function forcing.

$$\hat{\epsilon}_c(\Delta t) = \frac{2\Omega(k)}{k} \sqrt{\frac{\cos(\Omega(k)\Delta t) \pm \cosh(\gamma k^2 \Delta t)}{1 - \cos(\Omega(k)\Delta t)}} \quad (33)$$

We can also verify our result implicitly by plotting the neutral stability curves for several decreasing values of  $r_1$  and  $r_2$ . From figure 5 we can see that subharmonic tongues are in general centered about odd values of  $k$  while harmonic tongues are centered on even values of  $k$ .

Figure 5 also shows that as we decrease the values of  $r_1$  and  $r_2$  the harmonic tongues gradually disappear. Indeed this is the same result determined in both [4] and [6]. Interestingly enough our results are very similar to those obtained in [6] using a Fourier series approximation to alternating delta function forcing. Indeed in (a) we utilize  $r_1 = 0.25$  and  $r_2 = 0.25$  which is a close approximation to the first term of the Fourier series (a sinusoid). By shrinking the values of  $r_1$  and  $r_2$  we are essentially creating the same effect as adding additional terms to the Fourier series.

### 4.3 Instabilities with Larger $r$ Values

Having demonstrated that alternating square wave forcing can be utilized to approximate alternating delta function forcing we now turn our attention to investigating the effects of increasing the values of  $r_1$  and  $r_2$ . By increasing

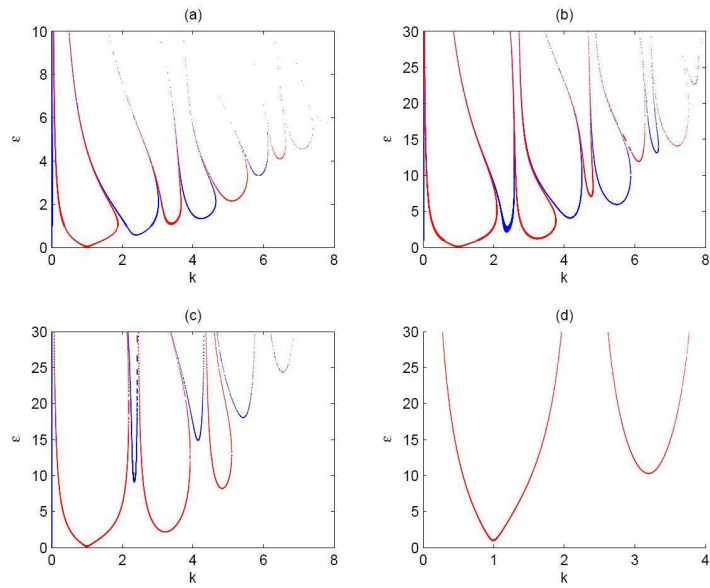


Figure 5: Square wave forcing designed to approximate alternating delta function forcing. Red corresponds to subharmonic tongues and blue corresponds to harmonic tongues. The ratios  $r_1$  and  $r_2$  as defined in (29) are as follows: (a)  $r_1, r_2 = 0.25$ , (b)  $r_1, r_2 = 0.1$ , (c)  $r_1, r_2 = 0.05$ , (d)  $r_1, r_2 = 0.01$ . Observe how the harmonic tongues continue to recede as the value of  $r_1$  and  $r_2$  are decreased. Note that the appearance of some tongues fading out is only an artifact of our numerical plotter and does not reflect their existence.

these values we are causing the system to spend more time either accelerating or decelerating. We begin by investigating what occurs when we maintain the condition that  $r_1 = r_2$  while increasing the  $r$  values. We then follow this up by investigating what occurs when we create a significant difference between the  $r$  values.

In this first experiment we maintain the condition that  $r_1 = r_2$ . By maintaining this condition, we cause the system to be constantly undergoing periods of acceleration followed by periods of deceleration back to zero velocity. Our first example involves using  $r$  values of 0.4. This provides a brief respite where the system maintains a constant velocity before undergoing the next acceleration. The effect of this forcing is that the minimum of both harmonic and subharmonic tongues gradually increases with wave number as may be seen in Figure 6(a). We also notice that harmonic tongues appear broader in comparison to the subharmonic tongues, contrary to the approximate alternating delta function forcing shown in the previous section. When we increase the  $r$  values to 0.49 as seen in Figure 6(b) we notice the same effects exaggerated.

Another interesting scenario to investigate involves what occurs when we remove the constraint  $r_1 = r_2$ . This then creates an asymmetry in the acceleration of the system. This implies that if  $r_1$  is larger, the system will have a net acceleration opposite the direction of gravity, while if  $r_2$  is larger, than the system will have a net acceleration in the same direction as gravity. When running these experiments we decided to utilize  $r$  values of 0.04 and 0.44 so that there are still extended periods of time with no acceleration, but there was a significant difference between  $r_1$  and  $r_2$ . In the first case shown in Figure 6(c) we see that  $r_1 = 0.44$  and  $r_2 = 0.04$ . This has the effect of increasing the width of the subharmonic tongues and shrinking the width of the harmonic tongues. It also decreases the growth rate of the minimum of each tongue. However, when we flip the  $r$  values some truly interesting behavior occurs as seen in Figure 6(d). In this circumstance we notice that the tongues have begun “pinching off” to form “islands.” In the sixth harmonic tongue this is particularly noticeable as the tongue is right at the onset of pinching. We also notice that minimum of the tongues increases extremely rapidly indicating that the system requires extremely large values of  $\epsilon$  to excite modes with even moderate  $k$  values.

## 5 Inverted Square Wave Forcing

From the results of the previous section, we noticed that very interesting instability patterns were arising when additional emphasis was placed on the  $-\epsilon$  component of the alternating square wave forcing. Based on this observation, we expected that similar behavior should also manifest itself in the case where we only had a  $-\epsilon$  component to the forcing. We used the same definition of square wave forcing as was presented in section 3, but instead inverted the forcing about the x-axis.

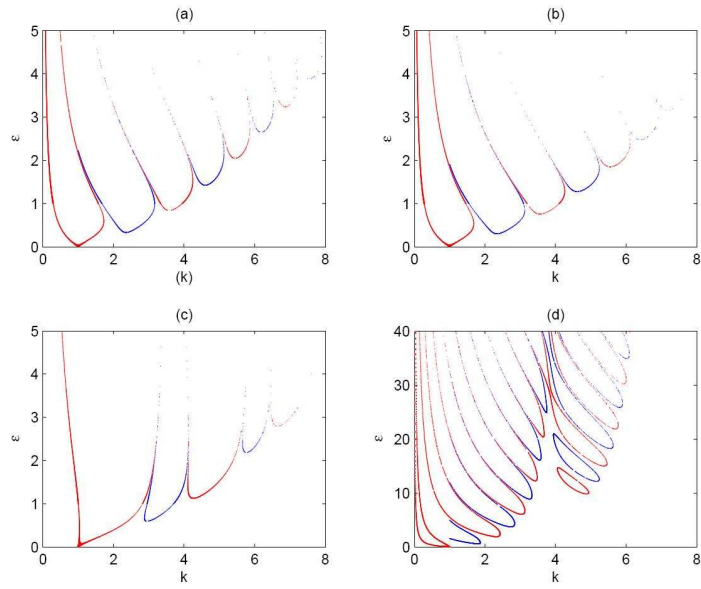


Figure 6: Square wave values corresponding to larger values of  $r_1$  and  $r_2$ . Red lines indicate subharmonic instabilities while blue lines correspond to harmonic instabilities. In the above examples the values of  $r_1$  and  $r_2$  as defined in (29) are as follows: (a)  $r_1, r_2 = 0.4$ , (b)  $r_1, r_2 = 0.49$ , (c)  $r_1 = 0.44, r_2 = 0.04$ , (d)  $r_1 = 0.04, r_2 = 0.44$ . Observe the creation of islands of instability when  $r_1 < r_2$ . Although the axis on the different plots different, increasing the axis range of (a)-(c) would not reveal any islands. Note that the appearance of some tongues fading out is only an artifact of our numerical plotter and does not reflect their existence.

In terms of the actual calculation itself, all of the equations are identical to those derived in section 3, except for (10b), which now has the form

$$\psi_\epsilon(t) = -\gamma k^2 \pm \sqrt{\Omega^2(k) + k\epsilon} \quad (34)$$

The same threshold condition that is described by (16) still applies and only the value of the  $\text{Tr}(M_k)$  will be modified. The same approximation to delta-function forcing derived in section 3.2 still holds as well.

We began our numerical analysis by again showing that we could approximate delta function forcing using small values of  $r$ . This can be seen in Figure 7(d) as the neutral stability curves are identical to those seen with delta function forcing. We also investigated slightly larger values of  $r$  up to  $r = 0.5$ . In the process of doing this we noticed that islands began forming even at values as small as  $r = 0.25$  as can be seen in Figure 7(b). This was very interesting as it indicated that very large values of  $r$  are not necessary to induce islands of instability.

After observing the impact of  $r$  values that were less than 0.5 we also wanted to examine the impact of  $r$  values that were greater than 0.5. We noticed that the increasing value of  $r$  had three effects that were different from the smaller values of  $r$ :

- There were no longer any islands for  $r \geq 0.6$  !
- As the value of  $r$  increases the tongues begin to compress in the sense that we are able to see more modes coming into play for smaller values of  $\epsilon$ .
- As the value of  $r$  increases the value of the minimum of a tongue increases for fixed  $k$ .

This result is particularly interesting as it indicates that additional acceleration, with decreased time to stabilize can actually result in fewer regions where patterns are likely to be excited. To understand this effect a more comprehensive analysis is necessary and will be discussed in the section on future work.

## 6 Impact of Fluid Parameters on Neutral Stability Curves

Having observed the existence of islands in the neutral stability curves, we wanted to better establish the conditions necessary for their presence. We have already discovered that islands form whenever inverted square wave forcing is the major component of the forcing function and the  $r$  value associated with the inverted square wave forcing component is within a certain threshold region. In this section we investigate the impact that varying the fluid parameters has

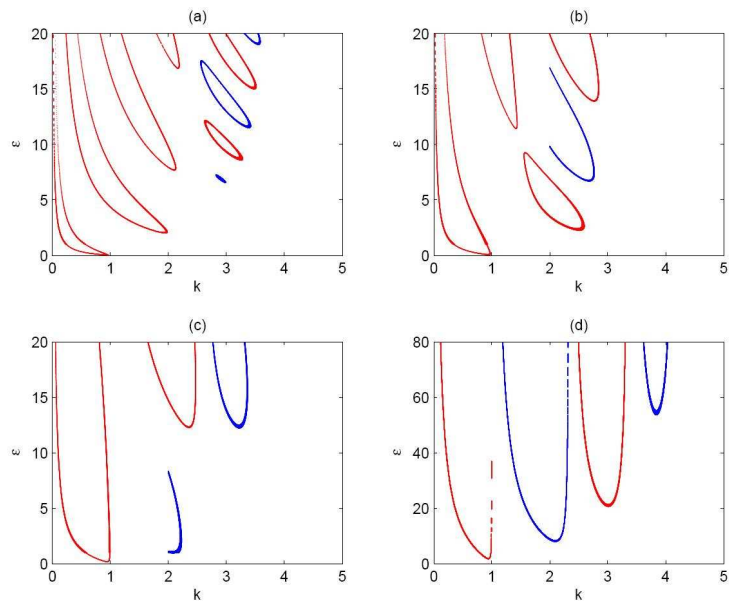


Figure 7: Neutral stability curves for square wave forcing designed to approximate delta function forcing with an inverted square wave. Red corresponds to subharmonic tongues and blue corresponds to harmonic tongues. The ratio of the square waves  $r$  as defined in (17) is (a)  $r = 0.5$ , (b)  $r = 0.25$ , (c)  $r = 0.1$ , and (d)  $r = 0.01$ . Note that the appearance of some tongues fading out is only an artifact of our numerical plotter and does not reflect their existence.

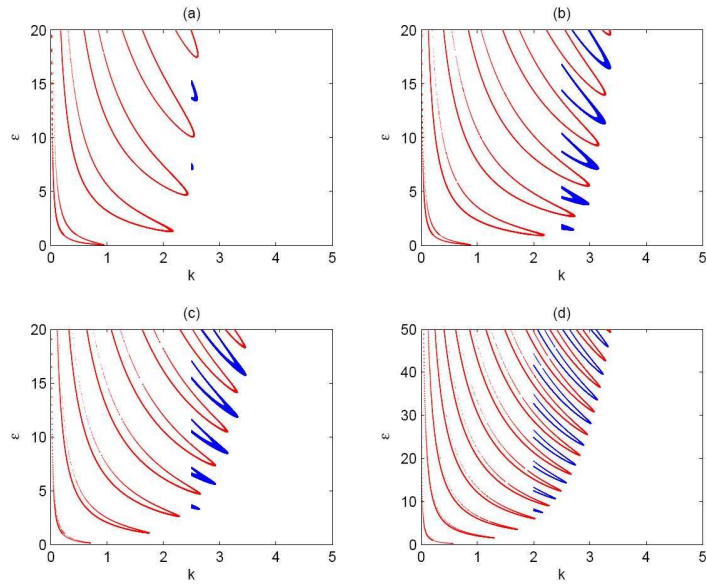


Figure 8: Neutral stability curves for square wave forcing with an inverted square wave and large values of  $r$ . Red corresponds to subharmonic tongues and blue corresponds to harmonic tongues. The ratio of the square waves  $r$  as defined in (17) is (a)  $r = 0.6$ , (b)  $r = 0.75$ , (c)  $r = 0.9$ , and (d)  $r = 0.95$ . Observe how the tongues continue to “pull up” rapidly, but do not form islands with larger values of  $r$ . Note that the appearance of some tongues fading out is only an artifact of our numerical plotter and does not reflect their existence.

on the formation of islands. We make use of the dispersion relation specified in (4) in order to vary the parameters. We used the inverted square wave forcing described in the previous section and varied the dimensionless fluid parameters such that one was emphasized more than the others.

### 6.1 Impact of $G_0$ and $\Gamma_0$

The first two fluid parameters that we investigate are  $G_0$  and  $\Gamma_0$ . We investigate these parameters together as they are directly related by the dispersion relation:

$$G_0 + \Gamma_0 = \frac{1}{4}. \quad (35)$$

Although both of these parameters are dimensionless, we can associate with them certain physical properties of the system. The parameter  $G_0$  can be associated with a constant acceleration that is being applied to the system. Intuitively this can be seen by noticing that in the damped Mathieu equation  $G_0$  occurs as a constant offset of the forcing function. Commonly this force is referred to as gravity, but it could also be used to describe some other force that is acting on the system and is co-linear with the direction of the forcing function. Similarly the dimensionless parameter  $\Gamma_0$  (defined in equation (3)) can be associated with the physical properties of the fluid and how resistant they are to change. Notice that for fixed  $k_0$  and  $\omega$ , large values of  $\Gamma_0$  point to a large surface tension and small fluid density. Due to the combined influences of these two physical properties understanding the exact effect of  $\Gamma_0$  is difficult. However, after investigating numerically the effect of larger  $\Gamma_0$  we have been able to determine that larger values of  $\Gamma_0$  will be more conducive to stable patterns.

We first investigated a system with a large value of  $G_0$  and consequently a small value of  $\Gamma_0$ . We maintained a modest value of  $r = 0.5$  so that we would be within the range of island formation.

The result seen in Figure 9 demonstrates that the occurrence of islands is not prohibited by large values of  $G_0$ , however we do notice that the first few tongues do not exhibit any islands. This is a direct consequence of  $G_0$  opposing the forcing function in the damped Mathieu equation. In addition to this the large value of  $\Gamma_0$  indicates a lower surface tension and a higher density. This is conducive to preventing the formation of patterns at smaller values of  $\epsilon$ .

We then considered the opposite scenario, with a small value of  $G_0$  and a large value of  $\Gamma_0$ . We maintained the same value of  $r = 0.5$  within the range of island formation.

Figure 10 again demonstrates the effects that we observed in the previous example. Notice that with a much smaller value of  $G_0$  and a larger value of  $\Gamma_0$  we see islands forming on lower order tongues. Also notice how with a larger value

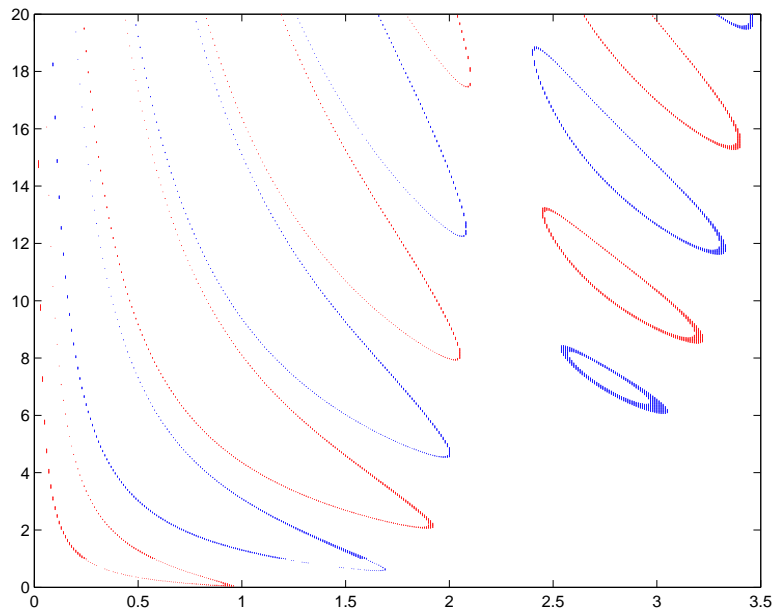


Figure 9: Neutral stability curves for inverted square wave forcing with  $r = 0.5$ . The fluid parameters are  $G_0 = 0.22$ ,  $\Gamma_0 = 0.03$ , and  $\gamma = 0.02$ . Observe how islands continue to form, even in the presence of a large value of  $G_0$ , but do not form on the lower order tongues. Note that the appearance of some tongues fading out is only an artifact of our numerical plotter and does not reflect their existence.

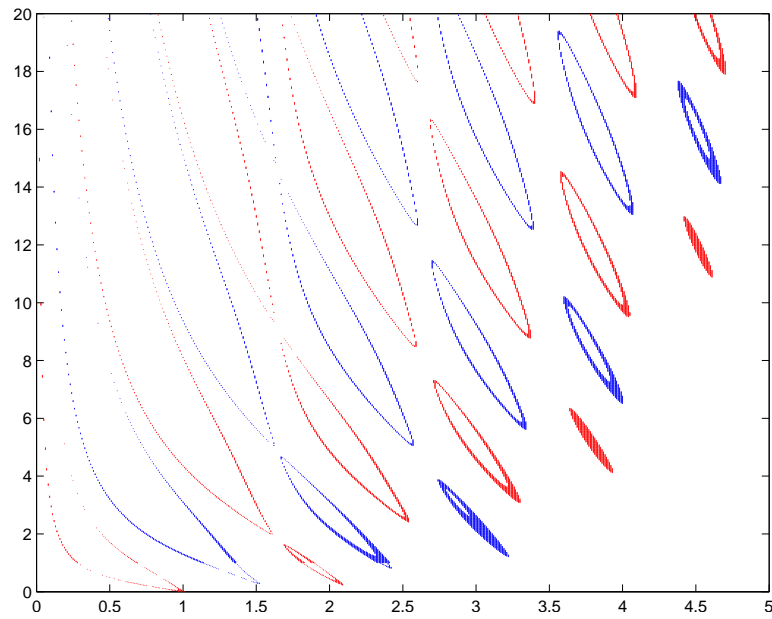


Figure 10: Neutral stability curves for inverted square wave forcing with  $r = 0.5$ . The fluid parameters are  $G_0 = 0.0395$ ,  $\Gamma_0 = 0.2105$ , and  $\gamma = 0.02$ . Observe in this example that large value of  $\Gamma_0$  and a small value of  $G_0$  are more conducive to forming islands on lower order tongues. Note that the appearance of some tongues fading out is only an artifact of our numerical plotter and does not reflect their existence.

of  $\Gamma_0$  the fluid has a higher potential for sustaining stable patterns which can be seen by the smaller minimum values of tongues as well as the occurrence of multiple islands along the same tongue.<sup>1</sup>

## 6.2 Impact of $\gamma$

The other dimensionless fluid parameter to be investigated in determining the presence of islands is  $\gamma$ . It is first important to observe two facts about  $\gamma$ : first, it is not dependent upon any dispersion relation and second, it occurs as a coefficient to both the first and zeroth derivative of the solution in the damped Mathieu equation. Intuitively this suggests that the  $\gamma$  parameter acts as a damping coefficient. This is also supported by the physical nature of  $\gamma$  being directly dependent upon the viscosity of the fluid being studied (3). Lower viscosity fluids will be more conducive to instability in pattern formation as a lower viscosity fluid will be more reactive to different modes of excitement, in both constructive and destructive manners.

We began by investigating  $\gamma$  by increasing its value. However, under these circumstances we noticed that no islands were occurring even with  $r = 0.5$ . We next examined what would occur as we decreased the value of  $\gamma$  while maintaining  $r = 0.5$  and choosing values of  $G_0$  and  $\Gamma_0$  that were NOT conducive to island formation as established in the previous section.

Figure 11 demonstrates extraordinarily surprising results as it shows numerous islands of stable patterns occurring for many different harmonic and subharmonic tongues! This indicates that with very small values of  $\gamma$  modes with  $k > 2$  can transition between stability and instability as forcing is increased. One last interesting conclusion that we drew from these results was that no islands would ever form on the first harmonic or subharmonic tongue unless the value of  $\gamma$  was reduced to 0 indicating a fluid with no viscosity. Whenever  $\gamma = 0$  the damped Mathieu equation reduces to a much simpler form:

$$\ddot{p}_k + [\Gamma_0 k^3 + (G_0 - G(t))k]p_k = 0 \quad (36)$$

How this equation allows for the formation of islands on the first subharmonic and harmonic tongues is an issue for further work that will be discussed in a later section.

## 7 Visualizing Pattern Formation

Having spent a great deal of time investigating the nature of the stability of patterns forming on the surface of the fluid, we wanted to observe the patterns created by square wave forcing. In order to do this we developed a numerical

---

<sup>1</sup>In order to verify that these conclusions were correct we investigated several other choices for the fluid parameters, but for purposes of space consideration we have not included them in this document.

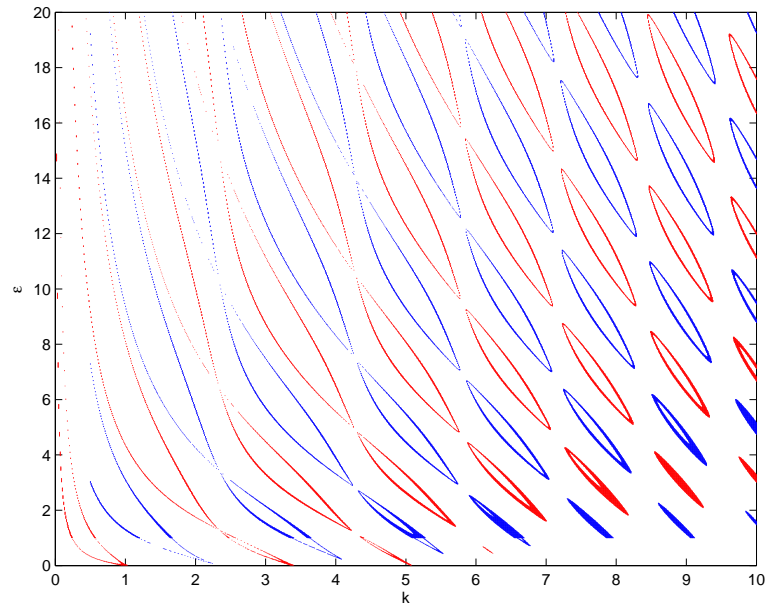


Figure 11: Neutral stability curves for inverted square wave forcing with  $r = 0.5$ . The fluid parameters are  $G = 0.2105$ ,  $\Gamma_0 = .0395$ , and  $\gamma = 0.0005$ . Observe that a small value of  $\gamma$  creates numerous islands on the same tongues, allowing for frequent transition between stable and unstable regions along the same mode. Note that the appearance of some tongues fading out is only an artifact of our numerical plotter and does not reflect their existence.

partial differential equations solver that could solve the Zhang-Viñal's equations in two dimensions and then plot the surface of the fluid. We begin by describing the numerical solver and then demonstrate the patterns that we captured for both square wave and alternating square wave forcing.

## 7.1 Numerical Methods

The numerical solver that we used is based on the solver described in [7]. We review here the basics of the pseudo-spectral method. We start with the Zhang-Viñal's equations except we replace the linear components with the label  $\mathcal{L}$  since these linear operators can be represented as matrices in our numerical method. We also replace the non-linear components with  $\mathcal{F}$  and  $\mathcal{G}$ , which are vectors, to find:

$$\partial_t h = \mathcal{L}_1 h + \mathcal{L}_2 \Phi + \mathcal{F} \quad (37)$$

$$\partial_t \Phi = \mathcal{L}_1 \Phi + \mathcal{L}_4(t) h + \mathcal{G}. \quad (38)$$

Here the linear operators are defined by

$$\mathcal{L}_1 = \gamma \nabla^2 \quad (39)$$

$$\mathcal{L}_2 = \hat{D} \quad (40)$$

$$\mathcal{L}_4(t) = \Gamma_0 \nabla^2 - G_0 + G(t). \quad (41)$$

In the next step we move the analysis into the frequency domain by taking the Fourier transform with respect to the spatial dimension. Note that this is why our method is referred to as pseudo-spectral as we perform our spatial analysis using spectral methods while our temporal component remains in the time domain. The equations can now be represented as:

$$\partial_t \hat{h}_k = \hat{\mathcal{L}}_1 \hat{h}_k + \hat{\mathcal{L}}_2 \hat{\Phi}_k + \hat{\mathcal{F}} \quad (42)$$

$$\partial_t \hat{\Phi}_k = \hat{\mathcal{L}}_1 \hat{\Phi}_k + \hat{\mathcal{L}}_4(t) \hat{h}_k + \hat{\mathcal{G}} \quad (43)$$

where the linear operators are defined as:

$$\hat{\mathcal{L}}_1 = -\gamma |\mathbf{k}|^2 \quad (44)$$

$$\hat{\mathcal{L}}_2 = |\mathbf{k}| \quad (45)$$

$$\hat{\mathcal{L}}_4(t) = -\Gamma_0 |\mathbf{k}|^2 - G_0 + G(t). \quad (46)$$

We now can discretize the problem in both the temporal and spatial dimensions. In order to do this we represent the time derivative as the definition of a derivative and use a trapezoidal method for the linear terms in the equation. For the non-linear components we apply a second order Adams-Bashforth method in order to ensure stability in our numerical method. We can then write the

equations as:

$$\begin{aligned} \frac{\hat{h}_k^{n+1} - \hat{h}_k^n}{\Delta t} &= \frac{1}{2}\hat{\mathcal{L}}_1(\hat{h}_k^{n+1} + \hat{h}_k^n) + \frac{1}{2}\hat{\mathcal{L}}_2(\hat{\Phi}_k^{n+1} - \hat{\Phi}_k^n) \\ &\quad + \frac{1}{2}(3\hat{\mathcal{F}}_k^n - \hat{\mathcal{F}}_k^{n-1}) \end{aligned} \quad (47)$$

$$\begin{aligned} \frac{\hat{\Phi}_k^{n+1} - \hat{\Phi}_k^n}{\Delta t} &= \frac{1}{2}(\hat{\mathcal{L}}_4^{n+1}\hat{h}_k^{n+1} + \hat{\mathcal{L}}_4^n\hat{h}_k^n) + \frac{1}{2}\hat{\mathcal{L}}_1(\hat{\Phi}_k^{n+1} - \hat{\Phi}_k^n) \\ &\quad + \frac{1}{2}(3\hat{\mathcal{G}}_k^n - \hat{\mathcal{G}}_k^{n-1}). \end{aligned} \quad (48)$$

After performing some algebra and solving for  $\hat{h}_k^{n+1}$  and  $\hat{\Phi}_k^{n+1}$  we find that we can write

$$\hat{h}_k^{n+1} = P(R_1 + M_1^{-1}M_2R_2) \quad (49)$$

$$\hat{\Phi}_k^{n+1} = P(M_4^{n+1}M_1^{-1}R_1 + R_2) \quad (50)$$

where the above are defined as

$$M_1 = 1 - \frac{\Delta t}{2}\hat{\mathcal{L}}_1 \quad (51)$$

$$M_2 = \frac{\Delta t}{2}\hat{\mathcal{L}}_2 \quad (52)$$

$$M_7 = 1 + \frac{\Delta t}{2}\hat{\mathcal{L}}_1 \quad (53)$$

$$M_4^n = \frac{\Delta t}{2}\hat{\mathcal{L}}_4(t) \quad (54)$$

$$M_4^{n+1} = \frac{\Delta t}{2}\hat{\mathcal{L}}_4(t + \Delta t) \quad (55)$$

$$R_1 = M_7\hat{h}_k^n + M_2\hat{\Phi}_k^n + \frac{\Delta t}{2}(3\hat{\mathcal{F}}_k^n - \hat{\mathcal{F}}_k^{n-1}) \quad (56)$$

$$R_2 = M_7\hat{\Phi}_k^n + M_4\hat{h}_k^n + \frac{\Delta t}{2}(3\hat{\mathcal{G}}_k^n - \hat{\mathcal{G}}_k^{n-1}) \quad (57)$$

$$P = (M_1 - M_4^{n+1}M_1^{-1}M_2)^{-1}. \quad (58)$$

Please note that the exponent  $X^{-1}$  in  $P$  does not refer to the reciprocal of the operator, but rather the inverse of the operator. Using MATLAB and the above equations we were able to code a numerical solver to simulate the surface of the fluid. After performing some initial experiments with our solver, we discovered that the error of our numerical method was extremely high. We then employed several of the methods described in [7] to reduce the effects of this error such as adding a low pass filter to remove noise from higher frequencies and zeroing the zero-wavenumber component on a regular basis. Both of these techniques allowed our simulations to run for much longer periods of time and accumulate significantly less error. We now describe the results that we observed by using our numerical solver to simulate the surface of a fluid under different square wave forcing functions.

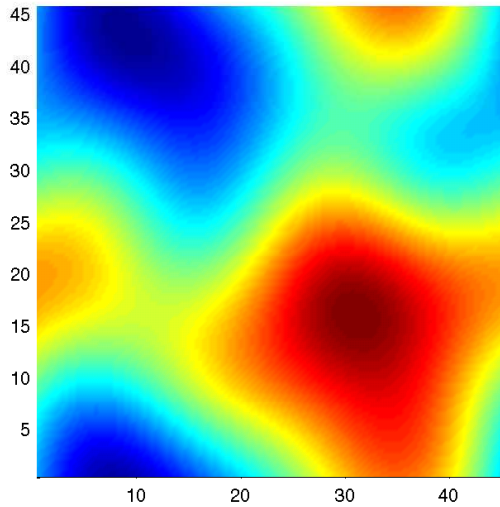


Figure 12: This is a pattern that was observed under square wave forcing with  $k = 1.1$ ,  $\epsilon = 0.5$ ,  $r = 0.5$ . Red corresponds to a higher amplitude and blue corresponds to a lower amplitude.

## 7.2 Patterns Arising from Square Wave Forcing

In order to observe patterns we first had to choose values for  $k$  and  $\epsilon$  that are within the stable pattern regions we observed in the neutral stability curves. One important aspect to this decision is that we must choose values of  $\epsilon$  that are small enough to only excite the first mode or possibly the first two modes. This is necessary to reduce the impact of interference of different frequencies on the formation of the pattern so that we only see the pattern explicitly associated with the first mode.

We began by examining a case with square wave forcing with  $k = 1.1$  and  $r = 0.5$ . Note from figure 2(a) that this is just inside the first sub-harmonic tongue and below the threshold for the first harmonic tongue. The pattern that we observed can be seen in figure 12.

We noticed that this pattern was not especially well formed, but after many cycles of forcing it remained persistent. We also noticed that it was not temporally static as can be seen in figure 13. Instead the peaks and valleys moved in circular motions with respect to each other. This is the cause for the poorly formed boundaries between the different nodes. From this we were able to see that unlike previous forcing functions, square wave forcing generates patterns that are stable, but not static.

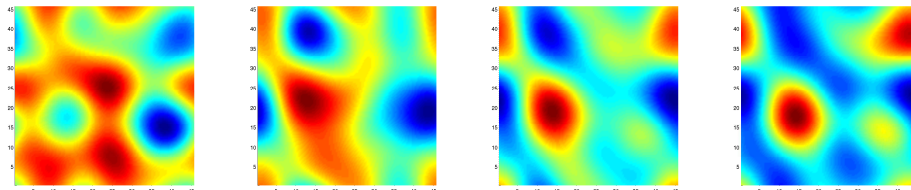


Figure 13: This figure shows the formation of several nodes over a small time frame with  $r = 0.15$ ,  $k = 1.1$ , and  $\epsilon = 0.5$ . Each frame is separated by 4 time steps in our numerical method. Notice how different nodes form and also move across the surface of the fluid.

The next step that we took was to observe the patterns that formed under inverse square wave forcing. We chose  $k = 0.9$  and  $\epsilon = 0.4$  consistent with the criteria that we determined for observing only the first wave mode. A snapshot of the pattern can be seen in figure 14.

In the case of this pattern, we noticed that the spatial boundaries of the pattern were better defined than the previous pattern. In addition to this the pattern seemed to be more temporally static, although not entirely. While the peaks and valleys would not migrate in the way that they did under square wave forcing, they would gradually flip amplitudes; that is valleys would transform into peaks and peaks would transform into valleys! This cyclic behavior was observed for all inverse square wave forcing. Another interesting thing to note was that the pattern did not appear to be of a multiple of the frequency  $T$  or  $T/2$  indicating neither a harmonic nor a sub-harmonic response. Investigating this result is a topic of future work. We were therefore able to conclude that both square wave forcing and inverse square wave forcing created patterns that are temporally dynamic, but entirely different in the nature of their dynamic behavior.

### 7.3 Patterns Arising from Alternating Square Wave Forcing

After investigating square wave forcing and inverted square wave forcing, we were interested to see what would occur under alternating square wave forcing where both forcing functions were present. For this experiment we chose values of  $r_1 = r_2 = 0.25$ ,  $k = 1.1$ , and  $\epsilon = 0.5$  based on figure 5(a) and the conditions set in the previous section. The pattern that we observed can be seen in figure 15.

Interestingly this pattern displayed characteristics of both of the patterns observed in the previous section. In this snapshot we notice that the fluid is divided into ridges. Like the previous patterns, this one was not temporally static either. Instead this pattern would constantly jump between the ridge-like

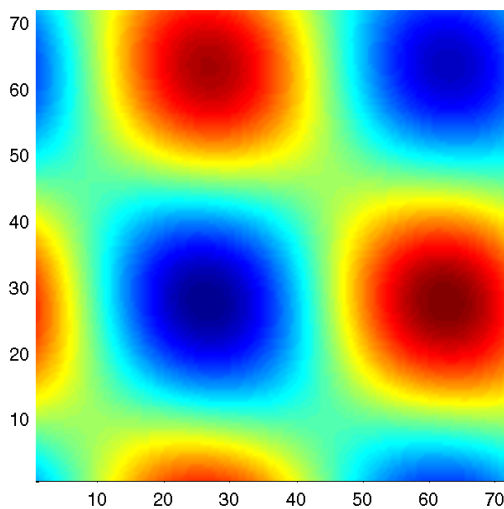


Figure 14: This is a pattern that was observed under inverse square wave forcing with  $k = 0.9$ ,  $\epsilon = 0.4$ , and  $r = 0.5$ . Red corresponds to a higher amplitude and blue corresponds to a lower amplitude.

pattern seen in figure 15 and the checkerboard pattern observed in figure 14. The most interesting part of this was that the ridges would form as a result of the peaks and valleys rotating into alignment with each other similar to the rotational movement observed in the pattern shown in figure 12. The peaks and valleys would then continue to rotate and transition until they returned to the checkerboard pattern. In this way, we noticed that both the square wave forcing and alternating square wave forcing were having an effect on the formation of the pattern in alternating square wave forcing.

#### 7.4 Understanding Pattern Formation Under Square Wave Forcing

Having observed the different patterns for square wave, inverted square wave, and alternating square wave forcing we were able to get a better feel for the stability and types of patterns that formed on the surface of the fluid. Unlike previous forcing functions that have been studied, square wave forcing didn't result in temporally stable patterns, but instead resulted in both spatially and temporally dynamic patterns. This is an interesting result that requires additional analysis that we discuss in the next section.

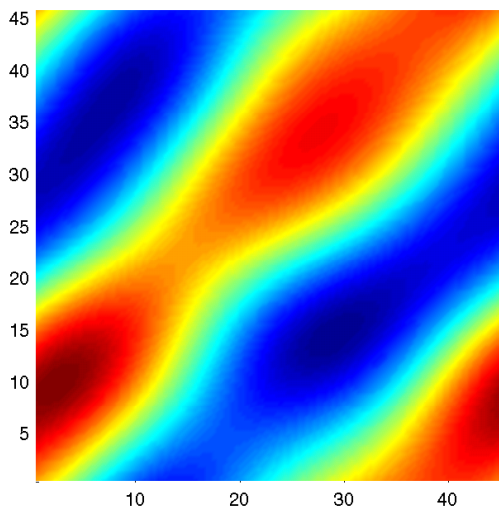


Figure 15: This is a pattern that was observed under alternating square wave forcing with  $k = 1.1$ ,  $\epsilon = 0.5$ , and  $r_1 = r_2 = 0.25$ . Red corresponds to locations of higher amplitude and blue corresponds to locations of lower amplitude.

## 8 Future Work

Although we have made a large step into investigating the stability and types of patterns generated by square wave forcing, there are still three open questions left by our work:

- What is causing the formation of islands in the neutral stability curves?
- Why do square wave forcing functions generate patterns that are different when alternating the sign of  $\epsilon$ ?
- Why does square wave forcing generate temporally dynamic patterns?

With regard to the first question we believe that the procedure for analyzing neutral stability curves has to be modified in order to incorporate information about the value of  $r$ . This is a direct result of the more general form of square wave forcing. Our hypothesis is that rather than having neutral stability curves in a two-dimensional space described by  $k$  and  $\epsilon$ , it will be necessary to describe neutral stability surfaces that are a function of  $k$ ,  $\epsilon$ , and  $r$ . In this sense the neutral stability curves that we observed in this work are simply cross sections of the actual neutral stability surfaces. This would help to explain the formation of islands as they are all part of the same surface, but are just not connected at individual values of  $r$ . We are still investigating whether this concept can be

used to explain the formation of islands.

With respect to the second question, we would expect to see the same behavior by the fluid regardless of the direction that it is being forced, but this is clearly not the case. Instead, we see marked differences in both the neutral stability curves and the patterns that form between the two different directions of forcing. Fortunately this effect has been observed in other forcing functions [6]. A weakly non-linear analysis can be used to better understand the cause of this behavior and should be another source of future work.

Lastly, square wave forcing clearly creates patterns that are temporally dynamic. This is different from many other forcing functions that have been observed that form temporally static patterns. The reason for this dynamic behavior is not clear from our current research and is certainly an open question to be investigated.

## 9 Conclusions

In this work we have investigated the effect of differing types of square wave forcing on pattern formation in Faraday systems. We have derived equations for the neutral stability curves and discovered the presence of islands of stability. Following the discovery of these islands of stability we attempted to better understand the different parameters that can lead to their formation. We noticed that inverted square wave forcing with moderate amounts of time spent accelerating often resulted in islands. We also investigated the effects of different dimensionless fluid parameters on the existence of these islands. Lastly, we developed a numerical solver for the Zhang-Viñal's partial differential equations in order to better determine the types of patterns that are generated by different types of square wave forcing.

## Acknowledgments

I would first and foremost like to thank my advisor, Anne Catllá, for all the encouragement and advice that she has given me over the past two years. The time that she has devoted both to this work, and to helping me discover where my true talents lie has been invaluable. A special thank you to Dr. Kraines for giving me the opportunity to pursue research in mathematics, the numerous get togethers at his house, and the chance to experience riding a Segway! I would also like to thank Matt Edwards and Kshipra Bhawalkar for their extensive contributions to my mathematical education: to Kshipra for always showing me that there are more elegant ways to think about things, and to Matt for always showing me that there are other things to think about. Finally, to Melissa Levy, for pushing me to make my math more rigorous, and my life less so.

## References

- [1] M. Faraday, Philos. Trans. Royal Society London **121**, 319 (1831).
- [2] W. Zhang and J. Viñals, J. Fluid Mech. **336**, 301 (1997).
- [3] D. W. Jordan and P. Smith, *Nonlinear Ordinary Differential Equations* (Oxford U.P., Oxford, 1999) 3rd ed. Chap. 9.
- [4] J. Bechhoefer and B. Johnson, Am. J. Phys. **64**, 1482 (1996).
- [5] E. D. Yorke, Am. J. Phys. **64**, 285 (1978).
- [6] A. Catllá and J. Porter and M. Silber, Phys. Rev. **72**, 056212 (2005).
- [7] Topaz, C. *Pattern Formation in Two Frequency Forced Faraday Waves* Ph.D. Thesis, Northwestern University (2002).
- [8] H. Arbell and J. Fineberg, Phys Rev Lett. **81**, 4384 (1998).
- [9] J. Porter, C. M. Topaz, and M. Silber, Phys. Rev. E **70**, 066206 (2004).
- [10] W. S. Edwards and S. Fauve, Phys. Rev. E **47**, R788 (1993).
- [11] H. W. Müller, Phys. Rev. Lett. **71**, 3287 (1993).
- [12] H. Arbell and J. Fineberg, Phys. Rev. Lett. **85**, 756 (2000).
- [13] T.B. Benjamin and F. Ursell, Proc. R. Soc. London, Ser. A **225**, 505 (1954).
- [14] K. Kumar and L.S. Tuckerman, J. Fluid Mech. **279**, 49 (1994).